NASA Technical Memorandum 79259

SOME TEM OBSERVATIONS OF Al_2O_3 SCALES FORMED ON NiCrAl ALLOYS

J. Smialek
Lewis Research Center
Cleveland, Ohio

and

R. Gibala
Case-Western Reserve University
Cleveland, Ohio

Prepared for the
Gordon Conference on Corrosion
New London, New Hampshire, July 23-27, 1979

Some TEM Observations of Al_2O_3 Scales Formed on NiCrAl Alloys

by J. Smialek and R. Gibala*
National Aeronautics and Space Administration
Lewis Research Center
Cleveland, Ohio 44135

ABSTRACT

The microstructural development of Al_2O_3 scales on NiCrAl alloys has been examined by transmission electron microscopy. Voids have been observed within grains in scales formed on a pure NiCrAl alloy. Both voids and oxide grains grew measurably with oxidation time at 1100° C. The size and amount of porosity decreased towards the oxide-metal growth interface. It was postulated that the voids resulted from an excess number of oxygen vacancies near the oxide-metal interface. Short-circuit diffusion paths were discussed in reference to current growth stress models for oxide scales. Transient oxidation of pure, Y-doped, and Zr-doped NiCrAl was also examined. Oriented α-$(Al,Cr)_2O_3$ and $Ni(Al,Cr)_2O_4$ scales often coexisted in layered structures on all three alloys. Close-packed oxygen planes and directions in the corundum and spinel layers were parallel. The close relationships between oxide layers provided a gradual transition from initial transient scales to steady state Al_2O_3 growth.

SUMMARY

The microstructures of Al_2O_3 scales formed on NiCrAl alloys at 1100° C have been examined by transmission electron microscopy. Furnace oxidation exposures of 0.1, 1, and 20 hr were used. The structure of the 20 hr scale was studied at various levels within the thickness of the oxide. Oxides that formed after short times on alloys doped with Y or Zr were also examined.

Log-log plots of the oxide grain size near the gas surface revealed a $t^{0.2}$ time dependence, a somewhat lower rate than bulk Al_2O_3 materials. A considerable amount of intragranular porosity ($\sim 5\%$) was also observed near the gas surface. The total amount of porosity did not change appreciably with time, but the average void diameter increased as $t^{0.4}$. Within experimental accuracy, this time dependence agreed with that for a conventional particle coarsening law, that is, $t^{0.33}$. Since the voids were predominantly intraganular for the scale on pure NiCrAl, they were not effective in retarding grain growth by grain boundary pinning.

*Case Western Reserve University.

With increasing distance inward from the gas surface, both the total amount and the average size of the voids gradually decreased to the limits of detectability. A tentative model for void precipitation within the scale was presented: As the oxide-metal interface recedes, the equilibrium concentration of oxygen vacancies at a fixed position in the scale is reduced. This causes the present vacancy concentration to now be in excess of the new equilibrium value; eventual condensation into voids results.

Dislocations and low angle grain boundaries were also observed to some extent in the mature α-Al_2O_3 scale. However, it is believed that their occurrence was insufficient to allow for appreciable short-circuit outward diffusion of aluminum through the scale. This is in contradiction to a previous model of growth stress and spalling for α-Al_2O_3 scales. A modified approach based on aluminum grain boundary diffusion is briefly discussed.

A number of complex features were observed in the transient stages of oxidation at 0.1 hr. Layers of oriented cubic $Ni(Al,Cr)_2O_4$ spinel or γ-Al_2O_3 and rhombehedral α-$(Al,Cr)_2O_3$ were found. The close-packed planes and directions of the oxygen sublattice were parallel for the oriented oxide layers. Fine precipitates were also present in the oriented oxides. It was suggested that these orientation relationships and precipitates provided a mechanism for a continuous transition of both scale structure and composition from the initial Ni-rich nuclei to the final stable α-Al_2O_3. The initial oriented scale was probably the result of an epitaxial effect with the substrate. The epitaxial relationship was soon lost, as random α-Al_2O_3 nucleated at the oxide-metal interface. There was a great diversity of structures observed at 0.1 hr, due to different underlying metal phases or foil position within the multi-layered scale. As a result no difference in scale structure between pure or doped NiCrAl could be stated categorically.

INTRODUCTION

Examination of oxide microstructures has been an integral part of studies of oxidation processes. Optical and scanning electron microscopy have been useful in documenting the grain size and shape, oxide layers, and the surface topography of scales. Transmission electron microscopy is a useful adjunct to these techniques. It can provide crystallographic as well as morphological information on the scales, with the advantage of higher resolution. Thus, TEM studies of scales have been used to document epitaxial effects, nucleation kinetics, and precipitation within the scale. For example, incubation periods of oxide nucleation were found for low temperature, low pressure oxidation of Cu, Cu-Ni, Al, and Fe-Cr alloys (refs. 1, 2, 3 and 4). Also epitaxial nucleation relationships were studied in these alloys as well as in Zr & Ti (refs. 5 and 6). TEM studies of the transient oxidation of (Ni,Co,Fe)Cr,Al alloys showed that many oxides are initially

nucleated before continuous, "healing," rate controlling scales of Al_2O_3 or Cr_2O_3 are formed (ref. 4, 7 and 8). All of the above studies dealt with relatively thin oxide films which represent the initial oxidation events. Very little work has been done on the thicker scales resulting from the more severe thermal exposures common in engineering applications.

The formation of Al_2O_3 scales on MAl or MCrAl alloys is particularly interesting for study because of the wide use of these materials as oxidation resistant coatings on gas turbine blades. SEM studies of Al_2O_3 scales on undoped FeCrAl, NiCrAl and CoCrAl alloys have shown that the Al_2O_3 scale is severely rumpled and often detached from the metal (refs. 9, 10 and 11). Goligthtly, et al., have measured the extent of the rumpling and found that a 30% lateral growth of the oxide has occurred after 24 hr at 1200° C. Thus a tremendous growth stress exists in the Al_2O_3 scale. On the other hand, alloys doped with <1 w/o of oxygen-active elements such as Y, Sc, Hf, Zr, etc. form scales with little or no rumpling, which are extremely adherent during thermal cycling.

A possible origin of the lateral oxide growth and resultant growth stress has been suggested by Golightly, et al. (ref. 9) as the short-circuit diffusion of aluminum outwards. This outward cation flux coupled with the inward grain boundary diffusion of oxygen thus would allow some oxide formation within the scale and necessitates lateral growth. Dislocations in Al_2O_3 were suggested as these short-circuit paths for aluminum; aluminum grain boundary diffusion is thought to be minimal in studies of bulk Al_2O_3. It was believed that the role of Y in the doped alloys was to segregate to dislocations and block the cation pipe diffusion in Al_2O_3, thus preventing oxide growth within the oxide.

Growth stress in oxides is a common phenomenon and similar theories based on the importance of lateral growth and short circuit paths have been proposed for pure Cr (ref. 12) and pure Ni (ref. 13). These studies have suggested that anion inward grain boundary diffusion is the cause of the growth stress for a scale normally growing by cation outward bulk diffusion. An interesting question for all the growth stress theories is whether or not there is some structural manifestation of lateral growth, such as grain boundary oxide nucleation. Structural studies by TEM are necessary in the case of Al_2O_3 to confirm the existence of the proposed short circuit paths (dislocations).

This, then provides a general background for the present TEM study of Al_2O_3 scales on NiCrAl alloys. The purpose of the present study is to document some of the oxide structures that evolve during typical thermal exposures of an oxidation resistant coating alloy. An attempt will be made to discuss these structures in light of current models for Al_2O_3 scale growth and adherence.

The work will be presented in two parts. The first maps out changes in a mature Al_2O_3 scale with time and through the thickness of the scale. Only scales formed at 1100° C on only pure Ni-15Cr-13Al will be discussed. In the second part some of the details of transient oxidation occurring in the first few minutes of oxidation will be discussed for pure Ni-15Cr-13Al and for Y or Zr doped NiCrAl. These Cr and Al levels were chosen on the basis of excellent cyclic oxidation resistance as mapped by Barrett & Lowell (ref. 14). These alloys are basically four phase materials: a dispersion of fine α-Cr particles in primary β-NiAl dendrites with γ/γ' Ni/Ni_3Al interdendritic areas.

EXPERIMENTAL PROCEDURE

Tungsten electrode arc melted buttons were made from Ni 270 sheet, iodide Cr, and Al shot (all 99.99% pure). Slices 0.65 mm thick were cut from the ingots and 3 mm diameter discs were obtained by spark machining. The discs were annealed in argon 24 hr at 1100° C, sanded to 0.25 mm, metallographically polished, and thoroughly cleaned. For oxidation exposure, the discs were placed edge-on in a FeCrAlY specimen holder which had been preoxidized to form a thick Al_2O_3 film to avoid contamination of the discs. The holders were also preheated to minimize heat-up time after lowering into the tube furnace. The furnace temperature was controlled to 1100° C ± 2° C. After exposure the specimens were cooled to room temperature in less than 5 minutes. Spalled oxides were directly ion thinned and examined in TEM. Discs with adherent oxides were carefully sanded with 600 grit paper on one side and electropolished from that side until perforation occurred. The remaining oxide overhanging the perforation was then ion thinned. Thus, all foils were in the plane of oxidation. TEM studies were done at 100 kV in a JEM-7A microscope employing a 360 degrees rotation ±20 degrees tilt specimen stage.

RESULTS

A. Pure Ni-15Cr-13Al at 1100° C

1. Effect of oxidation time

The scales formed on pure NiCrAl were primarily α-Al_2O_3. At short oxidation times (0.1 hr) some areas were found where preferred orientations of α-Al_2O_3 and $NiAl_2O_4$ spinel existed. This will be discussed in part B. Randomly oriented α-Al_2O_3 was also commonly observed in other areas of the 0.1 hr scale, figure 1.

The predominant features of the random Al_2O_3 scale at 0.1 hr is a widely varying lateral grain size 0.05 to 0.20 μm, with an average of 0.12 μm. There is also a dispersion of fine, nearly equiaxed voids about 100 A in diameter. After 1 hr (fig. 2) the average grain size increased to 0.18 um and the voids have coalesced to 280 A. And

at 20 hr the grains near the gas surface of the scale have grown to 0.33 μm (fig. 3(b)). The voids have coarsened to such an extent that only about one void per grain remains, with an average diameter of 950 A.

The kinetics of grain and void growth are shown graphically in figure 4. The grain diameter followed a $kt^{0.2}$ relationship for the oxide structure in the outer layer of the scale. SEM studies of Al_2O_3 grain growth at the inner layer also showed a $kt^{0.2}$ relationship for NiAl oxidized at 1100° C (ref. 15, Smialek). The Al_2O_3 grain size was determined from SEM and TEM photos of the oxide-gas surface also for a Pt_2Al phase oxidized at 1200° C (ref. 16). It was found that a $kt^{0.25}$ relationship held. The lateral grain growth of Al_2O_3 scales in the 1100° to 1200° C range thus follows a $t^{0.2-0.3}$ growth law and the time-exponent appears to be somewhat independent of alloy composition.

Theoretical models of unimpeded grain growth in crystals predict a $d^2-d_o^2= kt$ relationship, where d_o is an initial grain size at t=o (ref. 17). For small d_o, a $d=kt^n$ relation results, where n=0.5. Experimentally, values of n= 0.1 to 0.3 are often obtained in a log-log plot of d vs t. Explanations for these low values of n are given in terms of increased grain boundary pinning effects at longer times, either by grain boundary precipitation or impurity segregation. Thus, the time-exponent of ~0.2 obtained here and for Al_2O_3 scales on other alloys is thought to result from segregation of insoluble impurities such as nickel or platinum. The grain boundary pinning by voids is not considered to be a sufficient explanation for the low time-exponent because there are very few voids decorating grain boundaries and the number of voids is actually decreasing with time.

The kinetics of void growth show a $t^{0.4}$ relationship. This bears some resemblance to the classic precipitate coarsening law describing Ostwald ripening (ref. 18). This theory states that the driving force for agglomeration is the reduction in total precipitate surface energy, and the predicted growth follows a $t^{0.33}$ law. This law is a possible model for the void growth shown in figure 4; the large variations in void size allow for some degree of uncertainty in the observed time-exponent of 0.4.

Estimates of the volume fraction of porosity made by point counting were 0.06, 0.04, and 0.07 (±40%) for the 0.1, 1, and 20 hr scales, respectively. It is thus established that no significant increase in the amount of porosity has occurred for the first-formed oxide layer (i.e., nearest the oxide-gas surface). Thus, the treatment of void growth as strictly a particle coarsening phenomenon, as opposed to some continuous vacancy injection and condensation process, is supported.

The ultimate origin of the voids at the gas-oxide surface then occurs during initial oxidation, i.e. at $t \leq 0.1$ hr. It would seem logical to postulate that the voids were simply spaces between the

first oxide nuclei that were left behind during subsequent grain growth. Indeed, entrapped porosity in sintered Al_2O_3 compacts is a well-established result of grain growth, albeit, exaggerated grain growth. Once the grains boundaries and voids are some distance apart, the rate of void removal by fast grain boundary diffusion is extremely low. However, the situation is not quite so simple. Porosity has been found to be forming anew, well below these first oxide nuclei. This phenomenon will be discussed in the following sections.

2. Microstructures at Various Locations in a Thick Scale

The changes in scale morphology with position in the scale are shown in figure 3 for a 20 hr scale. At the very oxide-gas interface blade-like protrusions of oxide were observed (fig. 3(a)). Such needles or blades were also observed in SEM studies of NiCrAl & NiAl alloys (ref. 11, 15 and 19). Large intragranular voids were also observed to extend through to the oxide-gas surface. The large voids persisted to some extent beneath the immediate surface and the oxide grains were more clearly visible because of the uniformity of the foil here (fig. 3(b)). The structure approximately midway into the scale is shown in figure 3(c). Here the porosity is on a much finer scale ($\sim$ 100 A) and the grain size is about twice that of the outer scale in figure 3(b). Clearly, fewer voids are being produced as the scale grows inward.

Many of the fine voids near the midsection of the scale are seen to have small dark particles associated with them (fig. 3(c)). These particles show stronger electron absorption than the surrounding Al_2O_3 and thus contain greater amounts of heavy elements, such as Cr or Ni. It is now illustrated that the possibility of elemental Ni metal may account for these particles. For the reaction:

$$2NiO + 4/3Al = 2Ni + 2/3\ Al_2O_3$$

$$\Delta G = -141\ 000\ CAL + RT\ \ln \frac{a_{Ni}^{\ 2}}{\left(a_{Al}\right)^{4/3}\left(a_{NiO}\right)^{2}}$$

The activity of aluminum in the vicinity of a void in α-Al_2O_3 near 1100° C has been calculated to be 3.0×10^{-10} (F. Kohl, unpublished research, NASA Lewis Research Center). This produces a negative free energy for the above reaction if

$$\left(\frac{a_{NiO}}{a_{Ni}}\right) \geq 2.3 \times 10^{-5}$$

Thus any NiO formed as a transient at the growth interface could be reduced to elemental nickel metal (a = 1) within the scale. The void surfaces may provide favorable sites for Ni nucleation and residence.

A schematic of the scale viewed in cross-section has been constructed (fig. 5) from the microstructures obtained at various levels in the scale. As the oxide-metal interface is approached, the grain size increases while the size and total amount of porosity is decreased. The very large intragranular voids extend through to the gas surface.

A few grains are naturally selected to accomplish scale growth; there apparently is not a continual re-nucleation process occurring at the oxide-metal interface. The large grains of the inner oxide are in agreement with SEM studies showing large, often columnar, Al_2O_3 grains at the oxide-metal interface.

3. A Mechanism of Void Precipitation

While void growth has been established as a simple particle coarsening phenomenon, the reason for void nucleation, especially near the inner layer of the scale, is not at all obvious. The gradient in the amount of total porosity through the scale suggests that the pAl & pO_2 gradients through the scale may be the cause of vacancy formation and precipitation into voids. The equilibrium concentration of ionic defects may be related to these partial pressures by the following hypothetical reactions (all reactions have been considered because of current disagreements on the major equilibrium defect species in pure and doped Al_2O_3):

1. $1/2\ O_2\ (vap) + 2e' = O_i''$ $\qquad K_1 = \dfrac{[O_i'']}{(pO_2)^{1/2}\ [e']^2}$

2. $1/2\ O_2\ (vap) + V_O^{\cdot\cdot} + 2e' = \phi$ $\qquad K_2 = \dfrac{1}{(pO_2)^{1/2}\ [V_O^{\cdot\cdot}]\ [e']^2}$

3. $Al\ (vap) = Al_i^{\cdot\cdot\cdot} + 3e'$ $\qquad K_3 = \dfrac{[Al_i^{\cdot\cdot\cdot}]\ [e']^3}{(pAl)}$

4. $Al\ (vap) + V_{Al}''' = 3e'$ $\qquad K_4 = \dfrac{[e']^3}{(pAl)\ [V_{Al}''']}$

Reactions (1) and (2) state that higher oxygen pressures (i.e., the oxide-gas surface) will increase oxygen interstitials and decrease oxygen vacancies. The Frenkel oxygen defect relation states that oxygen vacancies and interstitials are inversely related:

5. $[V_O^{\cdot\cdot}]\ [O_i''] = K_{F,O}$

Thus, regardless of whether (1) or (2) predominates, fewer oxygen vacancies will be in equilibrium at the high pO_2 gas surface than at the oxide-metal surface. From reactions (3) and (4) it can be seen that high aluminum equilibrium vapor pressures (i.e., at the oxide-metal interface) will increase aluminum interstitials or decrease aluminum vacancies. The Frenkel aluminum defect relation states that:

$$6. \quad \left[V'''_{Al}\right]\left[Al_i^{\cdot\cdot\cdot}\right] = K_{F,Al}$$

Thus, regardless of whether (3) or (4) predominates, fewer aluminum vacancies will be in equilibrium at the oxide-metal interface than at the gas surface.

Finally the oxygen and aluminum vacancies are inversely related by Schottky equilibrium:

$$7. \quad \left[V'''_{Al}\right]^3\left[V_o^{\cdot\cdot}\right]^2 = K_S$$

Irrespective of which defect equation predominates, oxygen vacancies will be greater at the oxide-metal surface and aluminum vacancies will be greater at the gas surface.

Gradients of equilibrium vacancy concentrations can be visualized as in figure 6(a). After further oxidation, the scale thickens (fig. 6(b)); but the equilibrium vacancy concentrations at the two interfaces remain the same; they are governed only by the fixed pO_2 (gas) and a_{Al} (metal). This has the consequence that at position "X", the equilibrium concentration of oxygen vacancies has dropped, while that of aluminum vacancies has been raised. The precipitation of unstable oxygen vacancies into voids is thus predicted for an inward growing scale. Furthermore, the amount of excess vacancies is less for deeper positions in the scale, as shown by the arrows at X_1, X_2, and X_3. This agrees qualitatively with the observation that the amount of porosity decreases towards the oxide-metal interface.

Obviously this simplistic model can not be accepted without further argument or verification. One serious difficulty is that total defect concentration in α-Al_2O_3 is likely to be very low at any oxygen pressure. Thus, it is difficult to explain in detail the production of $\sim$5% porosity by vacancy condensation. However, this difficulty would exist for other vacancy precipitation models as well. This model is thus presented as a tentative framework for further study.

4. Short-Circuit Aluminum Paths and Growth Stress

In addition to the void morphologies discussed above, a number of individual dislocations and dislocation networks were observed in the α-Al_2O_3 scale. Figure 7 shows a low angle grain boundary cutting

through a large alumina grain. At high magnification it can be seen that the boundary consists of a finely spaced 14 A wide Moire' pattern produced by a slight rotation of the adjoining crystals. From diffraction theory, $D = d_{hkl}/\beta$, where D is the spacing of the Moire' fringes, d_{hkl} the spacing of the reflecting Bragg planes, and β the angle of mismatch between subgrains (ref. 20). Thus, β was estimated to be $\sim 7^{o}$. Although, a number of these low angle boundaries were observed, it is difficult to determine the frequency with which they occurred. For example, for a given field of view, only some grains were oriented so as to produce the strong diffracting conditions required to image any dislocations present. (Because of the fine grain size, proper orienting of each grain was impossible). Very few of the diffracting grains showed any clear indication of dislocation structures. This can be seen by examining figures 1, 2, 3(b), and 3(c).

According to the growth stress model of Al_2O_3 spallation (ref. 9), aluminum outward diffusion via short-circuit paths, such as dislocations, forms new oxide within the existing scale causing a lateral growth. Consequently a large compressive stress is generated in the scale, causing buckling and ultimately spalling when the sample is cooled. The absence of a substantial number of dislocations in this scale (which did spall) leads one to look elsewhere for short-circuit paths for aluminum.

Grain boundaries were initially discounted because th y were believed to be inoperative in bulk polycrystalline alumina at 1670° to 1900° C (ref. 21). However, at 1100° C aluminum grain boundary diffusion could be significantly enhanced with respect to lattice diffusion of aluminum. Grain boundary oxide protrusions in Al_2O_3 scales at the gas surface (lace structure) were found for Pt-6Al, (ref. 16) and NiAl (ref. 15, Smialek, and Smeltzer, unpublished research, McMaster Univ., Ontario). This indicates that outward aluminum grain boundary diffusion may indeed be operative at 1100° C. Furthermore, evidence put forth by Paladino & Kingery against the significance of aluminum grain boundary diffusion was only that Al^{26} concentration profiles fit an analytial treatment based on bulk diffusion. No attempt to treat the profiles by a combined boundary + bulk diffusion model was made. The samples were also very large grained (130 μm) compared to the polycrystals where, for example, oxygen grain boundary diffusion was found to be important (ref. 22, 25 μm, Al_2O_3, Oishi & Kingery).

Thus, the growth stress model of Golightly, et al. may still apply if grain boundaries rather than dislocations are considered as the short circuit paths for aluminum. This is analogous to the stress model put forward by Rhines and Wolf (ref. 13) for oxidation of Ni and by Caplan and Sproule for Cr (ref. 12). It is not immediately clear how such a growth mechanism will necessarily be manifested in the microstructure. One might expect to see oxide nucleation at grain boundaries but this was not observed. Or one might expect to see an

accentuated widening of grains but this was not observed. The TEM studies have thus not provided much directly supportive evidence of the growth stress models.

B. Transient Oxide Scales Formed on NiCrAl + (Y) or (Zr) Alloys

In order to trace some of the mature oxide structures back to their origins, NiCrAl alloys were oxidized at 1100° C for only 0.1 hr. The effects of 0.5 w/o Y and Zr alloy dopants were also studied. What resulted was a myriad of new oxide structures, some of which bore little resemblance to those discussed in Part A. It is believed that the multiple oxide structures at short times resulted from the following causes: (1) Multiple underlying metal phases, i.e., β-NiAl and γ/γ'(Ni-Ni_3Al); (2) different positions in the scale, i.e., Ni & Cr-rich oxides formed initially at the gas surface as opposed to subsequent pure α-Al_2O_3 at the oxide-metal interface; and (3) complex relationships between oxide structure and uncontrolled parameters such as metal grain orientation or surface condition.

1. Randomly Oriented α-Al_2O_3

Figure 8 represents the microstructures characteristic of the α-Al_2O_3 scale with random grain orientations formed on the pure NiCrAl alloy. Fine pores and much intense strain contrast are present in nearly every grain. The randomly oriented α-Al_2O_3 was observed to be in intimate contact with the metal in many areas. In the areas of oxide-metal contact, the size and amount of porosity was much less than that shown in figure 1. Thus, even at 0.1 hr, a gradient in pore structure existed through the scale. This structure appears to be a direct antecedent of the mature α-Al_2O_3 structures referred to in part A. Randomly oriented α-Al_2O_3 was also observed on the Y and Zr-doped alloys with many of the same characteristics previously mentioned.

One of the distinct differences found in the scale formed on the Y-doped NiCrAl was the existence of substantial amounts of intergranular porosity (fig. 9). This porosity was noticed in areas of the scale having both random and preferred orientation (texture).

2. Oriented Scales

The preferred orientation of some oxide areas was evidenced by single crystal diffraction patterns corresponding to areas much larger than the random α-Al_2O_3 grain size. The pattern in figure 10 for Y-doped NiCrAl shows two coincident zones for α-$(Al,Cr)_2O_3$ and $Ni(Al,Cr)_2O_4$. The orientation relationships of the rhombehedral and cubic oxides are such that close-packed planes and directions of oxygen atoms are parallel. This feature is believed to provide a mechanism for direct growth of the α-Al_2O_3 inner layer from the initial transient spinel oxides. The schematic shows the similarity of possible cubic [111] and rhombehedral [0001] zones. Inspection of the inner ring of spots, however, establishes unequivocal differentia-

tion between these three oxides. The calculated position of NiO reflections is also shown in the schematic, but these were not observed. The values of the lattice parameters indicated the presence of substantial amounts of Cr in solution in both the corundum and spinel structures.

Oriented scales were observed on all three alloys, with a higher degree of orientation for the Y-doped and especially for the Zr-doped NiCrAl. The Zr-doped NiCrAl showed the same close-packed orientation relations as in figure 10; however, the two phases were α-$(Al,Cr)_2O_3$ and γ-Al_2O_3. The oriented scales were probably the result of epitaxial growth relations between the oxide and metal substrate. These relations could not be studied on the 0.1 hr scales because an inner layer of random α-Al_2O_3 had already formed. Thus there were no areas where both oriented oxide and metal diffraction patterns could be obtained. Oriented or textured scales have been observed previously in transient oxidation of NiCrAl alloys, but again exact relationships with the metal substrates were not studied (refs. 8 and 23).

The general structure of the oriented scales was that of fine, 0.1 μm subgrains arranged in a layered fashion. Thus Moire' patterns and strain contours were often produced by the interface of coherent layers of subgrains. An example of the strained subgrain structure is shown in figure 11 for a γ-Al_2O_3* scale on the Zr-doped alloys. Higher magnification (fig. 12) reveals a dense network of precipitates (P) and finely spaced Moire' fringes (M), all showing a distinct crystallographic orientation. A precipitate morphology based on $\{111\}$ $\langle 110\rangle$ narrow blades (fig. 13) accounts for the various precipitate and Moire' directions observed. Since γ-Al_2O_3 is a highly defective spinel structure, it is believed that the Widmanstatten precipitates represent a transition phase between γ and α-Al_2O_3. Transition phases occurring on close-packed $\{111\}$ planes and aligned along closepacked $\langle 110\rangle$ directions are typical for spinel-to-corundum transformations in bulk materials. Some precipitation in the oriented α-$(Al,Cr)_2O_3$ scales on the pure and Y-doped alloys was also observed. However, in these cases the precipitate is expected to be the cubic structure (or spinel) rather than another rhombehedral phase.

Another interesting feature of the γ-Al_2O_3 defect spinel scale formed on the Zr-doped alloy were anti-phase domain boundaries (fig. 14). These boundaries separate regions of spinel where the cation ordering has become out of phase. Such an occurrence can occur easily in spinel structures because the oxygen sublattice remains intact across the (APB'S). Extra reflections in parts of the γ-Al_2O_3 scale indicated the presence of some special ordering phenomenon (fig. 15). Two subcells in reciprocal space were found to exist within the standard spinel pattern, namely $1/2\ \bar{g}\ (11\bar{1})$,

* The existence of γ-Al_2O_3 has been reported in the literature for pure Al and Ni-Al alloys at temperatures less than 800° C (refs. 3, 7, 24 and 25). It is thus beleved that the γ-Al_2O_3 scale observed here represents a metastable transient form of alumina.

1/3 $\bar{g}$ ($3\bar{1}1$) and 1/2 $\bar{g}$ ($1\bar{1}1$), 1/3 $\bar{g}$ ($31\bar{1}$). While lower symmetry decomposition phases between spinel and corundum structures have been reported, none were found which could give rise to these specific extra reflections. Apparently another metastable transition phase between γ and α-Al_2O_3 has formed here. The extra reflections could not be attributed to the fine precipitates previously discussed.

A schematic of an oxide cross-section after 0.1 hr at 1100° C is shown in figure 16. While three distinct layers are shown here to depict the full sequence of oxidation, it is emphasized that in any one area all structures may not be present. The Ni and Cr-containing layers are probably the first scales to form, since transient oxides most closely resemble the composition of the alloy. (This is the model presented by Giggins & Pettit and Kear, et al., refs. 26, 8). The subgrain structure of the oriented scales contain many fine features such as precipitates, Moire' patterns, and APB'S. These can be related to transitions between layers. Finally, only the stable α-Al_2O_3 is observed in intimate contact with the metal substrate, at least in areas where metal was observed. The random α-Al_2O_3 is thus concluded to be the inner oxide scale. Voids were present in all layers, and were noticeably less prevalent at the oxide-metal interface. This is in accord with the absence of voids at the oxide-metal interface for mature α-Al_2O_3 scales (Part A).

3. Relation of Initial Transient Scales to Stable α-Al_2O_3

Some insights on the development of mature oxide structures have been gained through the study of transient oxidation. Voids were observed in the various oxide layers well below the initial scale surface (oxide-gas surface). This supports the contention that voids were not simply the result of gaps left between the initial oxide nuclei on the fresh metal surface. Some process continuing beneath the original oxide layer, such as the condensation of non-equilibrium oxygen vacancies proposed in Part A, appears to be more tenable.

The orientation relationships among the $Ni(Al,Cr)_2O_4$, γ-Al_2O_3, and α-$(Al,Cr)_2O_3$ layers can be viewed as a mechanism to provide a structural and compositional continuum between the transient oxide layers and α-Al_2O_3. The tendency toward Widmanstatten precipitation observed in the oriented layers is another manifestation of the orientation relationship between the phases. It is not known why the random α-Al_2O_3 is preferred as the stable mature oxide rather than an oriented oxide of the same composition and structure.

It is recognized that the subgrains found in the mature random α-Al_2O_3 (part A) may have resulted from the subgrains formed during initial oxidation in the oriented oxide layers. However, it is difficult to envision a distinct correlation between a few subgrains

in a random 0.5 μm grain size layer and a fully oriented layer filled with 0.1 μm subgrains. The subgrains in the mature scale may simply have resulted from the growth stresses in scale.

CONCLUDING REMARKS

While the TEM study revealed a number of new features of Al_2O_3 scales, their full impact on oxidation mechanisms will not become evident without further study. For example, the transient oxide scales on the pure NiCrAl did not show definitive structural differences from those on alloys doped with Y or Zr (adherence additives). Thus there was no insight gained towards adherence mechanisms based on structural evidence. On the contrary, the lack of dislocation structures in the mature Al_2O_3 scales on the pure NiCrAl did not support a previous growth stress theory of oxide spalling. Mature oxide structures on the Y and Zr-doped alloy should thus continue to be studied in detail in addition to the transient scales.

The initial oriented oxides strongly suggested an epitaxial effect. The epitaxial relationships with the metal should be studied directly with the ultimate goal of finding conditions to prolong epitaxy (and probably adherence). Single crystal and in-situ TEM experiments are better suited for this type of work.

REFERENCES

1. Heinemann, Klaus; Rao, D. B.; and Douglass, D. L.: Oxide-Nucleation on Thin Films of Copper During in Situ Oxidation in an Electron Microscope, Oxid. Met., vol. 9, no. 4, 1975, pp. 379-400.

2. Heinemann, Klaus; Rao, D. B., and Douglass, D. L., In Situ Oxidation Studies on (001) Copper-Nickel Alloy Thin Films. Oxid. Met., vol. 11, no. 6, 1977, pp. 321-334.

3. Scamans, G. M.; and Butler, E. P.: In Situ Observations of Crystalline Oxide Formation During Aluminum Alloy Oxidation. Met. Trans., vol. 6A, Nov. 1975, pp. 2055-2063.

4. Howes, V. R., The Early Growth of Oxide on a Fe-Cr Alloy," Corros. Sci., vol. 7, no. 11, 1967, pp. 735-746.

5. Ploc, R. A.: Transmission Electron Microscopy of α-ZrO_2 Films Formed in 573 K Oxygen. J. Nucl. Mater., vol. 61, no. 1, 1976, pp. 79-87.

6. Flower, H. M.; and Swann, P. R.: An in Situ Study of Titanium Oxidation by High Voltage Electron Microscopy. Acta. Met., vol. 22, Nov. 1974, pp. 1339-1347.

7. Wood, G. C.; and Chattopadhyay, B.: Transient Oxidation of Ni-Base Alloys. Corros. Sci., vol. 10, no. 7, 1970, pp. 471-480.

8. Kear, B. H.; et al.: On the Transient Oxidation of a Ni-15Cr-6Al Alloy. Oxid. Met., vol. 3, no. 3, 1971, pp. 557-560.

9. Golightly, F. A.; Stott, F. H., and Wood, G. C.: The Influence of Yttrium Additions on the Oxide-Scale Adhesion to an Iron-Chromium-Aluminum Alloy. Oxid. Met., vol. 10, no. 3, 1976, pp. 163-187.

10. Tien, J. K.; and Pettit, F. S.: Mechanism of Oxide Adherence on Fe-25Cr-4Al (Y or Sc) Alloys. Met. Trans., vol. 3, June 1972, pp. 1587-1599.

11. Giggins, C. S.; and Pettit, F. S.: Oxide Scale Adherence Mechanisms and the Effects of Yttrium, Oxide Particles and Externally Applied Loads on the Oxidation of NiCrAl and CoCrAl Alloys. PWA-5364, Pratt & Whitney Aircraft, 1975. (ARL-TR-75-0234), AD-A024104.)

12. Caplan, D.; and Sproule, G. I.: Effect of Oxide Grain Structure on the High-Temperature Oxidation of Cr. Oxid. Met., vol. 9, no. 5, 1975, pp. 459-472.

13. Rhines, F. N.; and Wolf, J. S.: The Role of Oxide Microstructure and Growth Stresses in the High-Temperature Scaling of Nickel. Met. Trans., vol. 1, June 1970, pp. 1701-1710.

14. Barrett, Charles A.; and Lowell, Carl E.: Resistance of Ni-Cr-Al Alloys to Cyclic Oxidation at 1100° and 1200° C. Oxid. Met., vol. 11, no. 4, 1977, pp. 199-223.

15. Smialek, James L.: Oxide Morphology and Spalling Model for NiAl. Met. Trans., vol. 9A, Mar. 1978, pp. 309-320.

16. Felten, E. J.; and Pettit, F. S.: Development, Growth and Adhesion of Al_2O_3 on Platinum-Aluminum Alloys. Oxid. Met., vol. 10, no. 3, 1976, pp. 189-223.

17. Kingery, W. D.; Bowen, H. K.; and Uhlmann, D. R.: Introduction to Ceramics. Second ed. John Wiley and Sons, Inc., 1976, p. 454.

18. Greenwood, G. W.: The Growth of Dispersed Precipitates in Solutions. Acta Met., vol. 4, no. 3, May 1956, pp. 243-248.

19. Smeggil, G. W.; and Bornstein, N. S.: The Effect of NaCl on the Oxidation of NiAl. J. Electrochem. Soc., vol. 125, no. 8, Aug. 1978, pp. 1283-1290.

20. Edington, J. W.: Philips Tech. [illegible]: Monograph in Practical Electron Microscopy in Mat[illegible]Science, 3, MacMillian (London), 1975, p. 82.

21. Paladino, A. E.; and Kingery, W. D.: Aluminum Ion Diffusion in Aluminum Oxide. J. Chem. Phys., vol. 37, no. 5, Sep. 1962, pp. 957-962.

22. Oishi, Y.; and Kingery, W. D.: Self-Diffusion of Oxygen in Single Crystal and Polycrystalline Aluminum Oxide. J. Chem. Phys., vol. 33, no. 2, Aug. 1960, pp. 480-486.

23. Koch, E. F.; and Romeo, G.: Growth of Thin Oxide Scales for Electron Microscopy Studies. Metallography, vol. 8, no. 6, Dec. 1975, pp. 509-514.

24. Fueki, K.; and Ishibashi, H.: Oxidation Studies on Ni-Al Alloys. J. Electrochem. Soc., vol. 8, no. 4, Apr. 1961, pp. 306-311.

25. Nazarova, R. I.: Electron Diffraction Study of the Oxidation Process of Thin Films of Intermetallic Compounds of the System Nickel-Aluminum. Izv. Akad. Nauk SSSR, Ser. Khim., no. 7, 1964, pp. 1164-1167. (Also NASA Translation TT F-10, 156, 1966.)

26. Giggins, C. S.; and Pettit, F. S.: Oxidation of Ni-Cr-Al Alloys Between 1000° and 1200° C. J. Electrochem. Soc., vol. 118, no. 11, Nov. 1971, pp. 1782-1790.

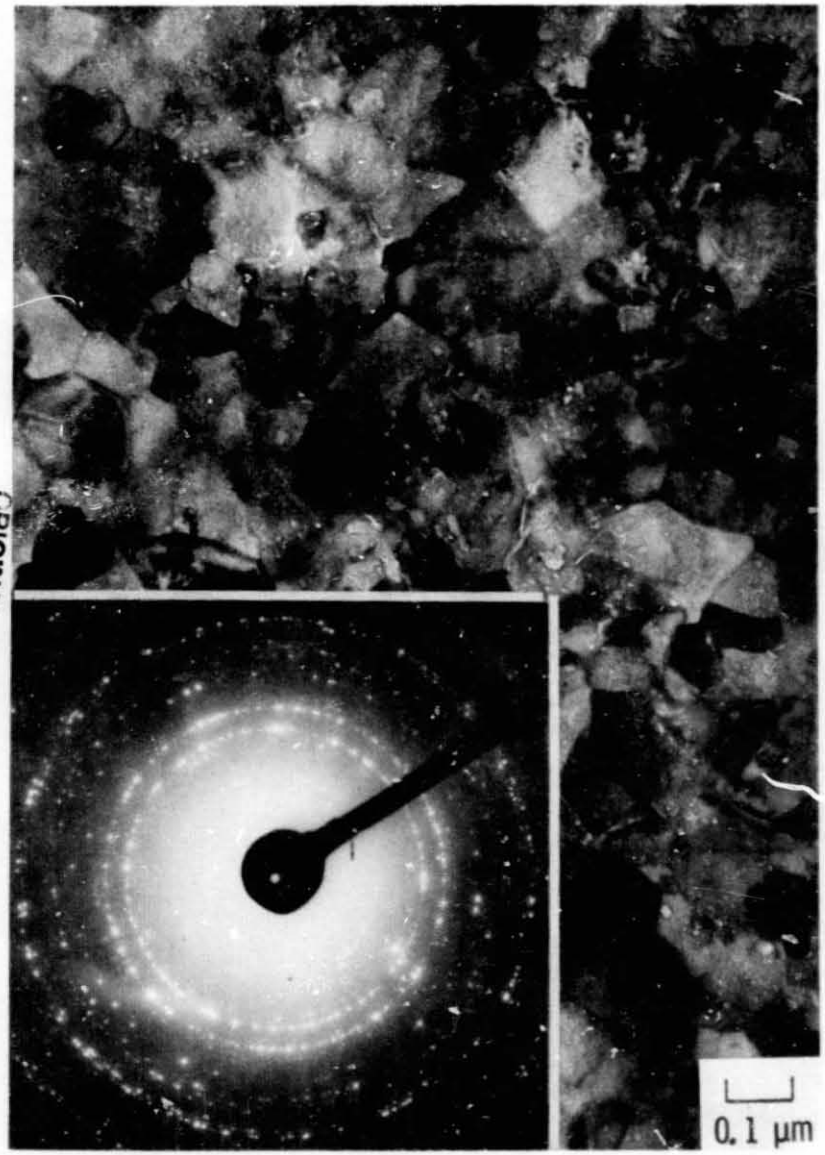

Figure 1. - Fine voids and grains in α - Al_2O_3 scale formed on pure NiCrAl, 0.1 hr at 1100° C.

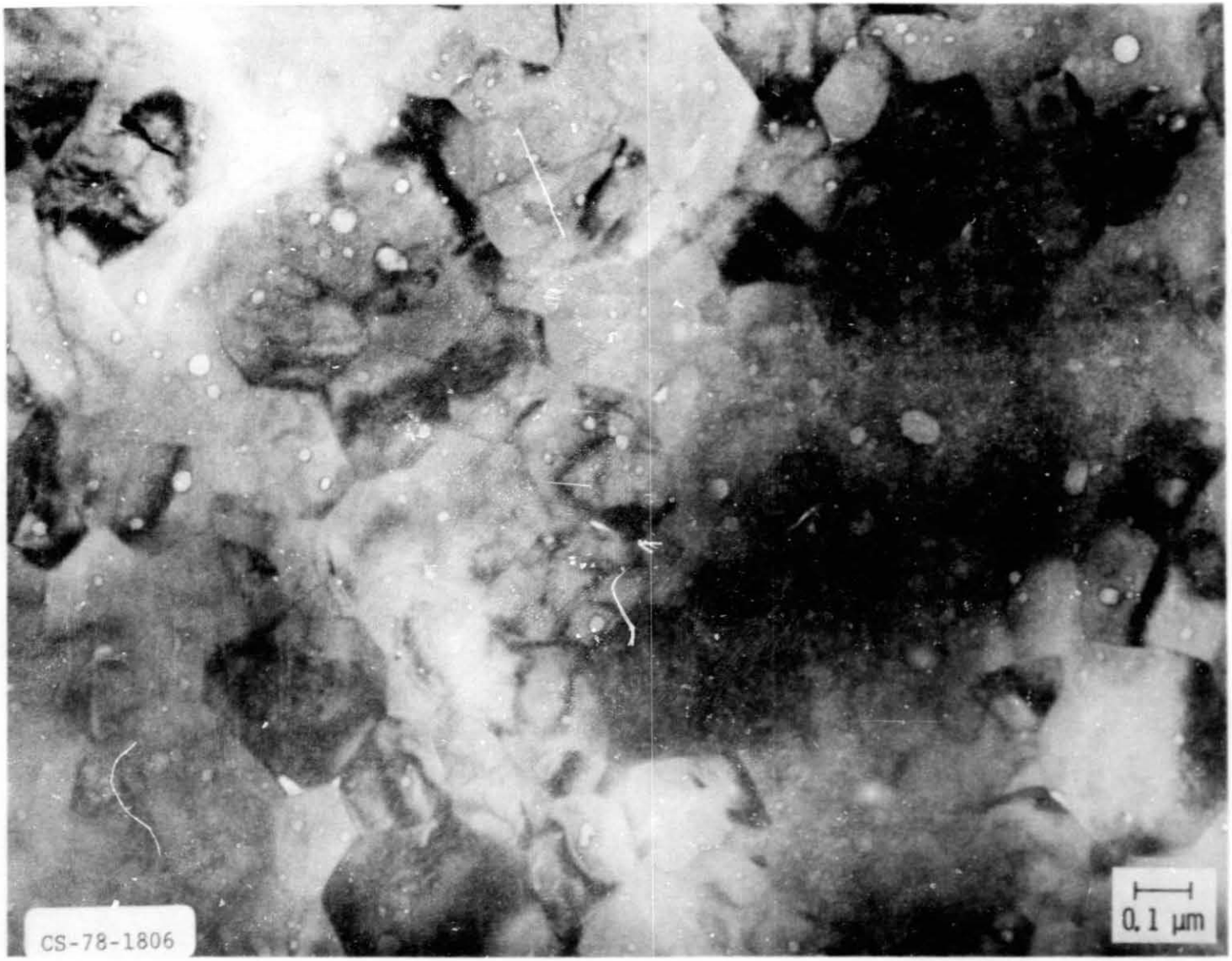

Figure 2. - Growth of voids and grains in $\alpha - Al_2O_3$ scale after 1 hr of oxidation.

(a) GAS-OXIDE INTERFACE.

(b) JUST BELOW GAS-OXIDE INTERFACE.

Figure 3. - Gradient in structure of $\alpha - Al_2O_3$ scale after 20 hr of oxidation.

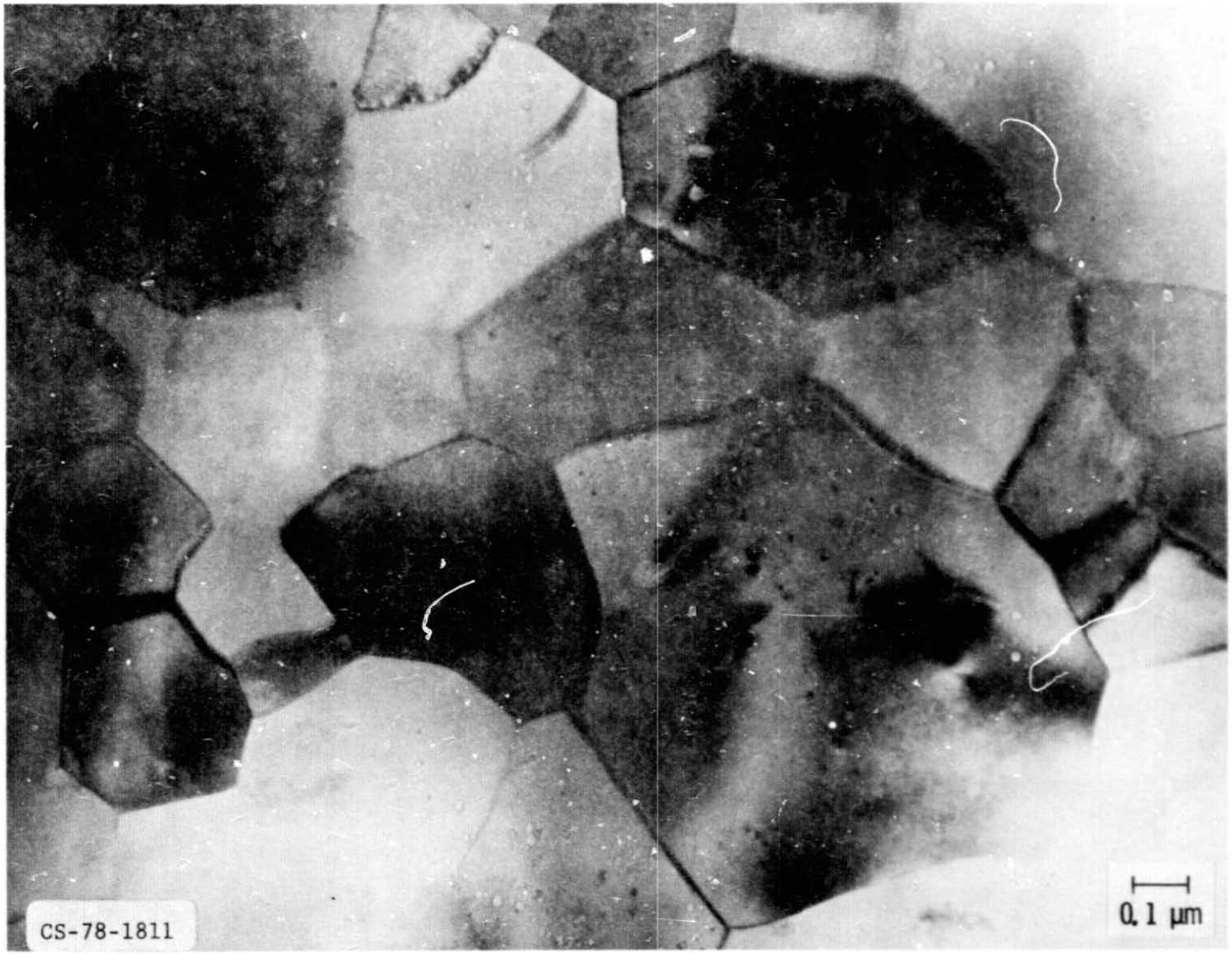

(c) NEAR MIDSECTION OF SCALE.

Figure 3. - Concluded.

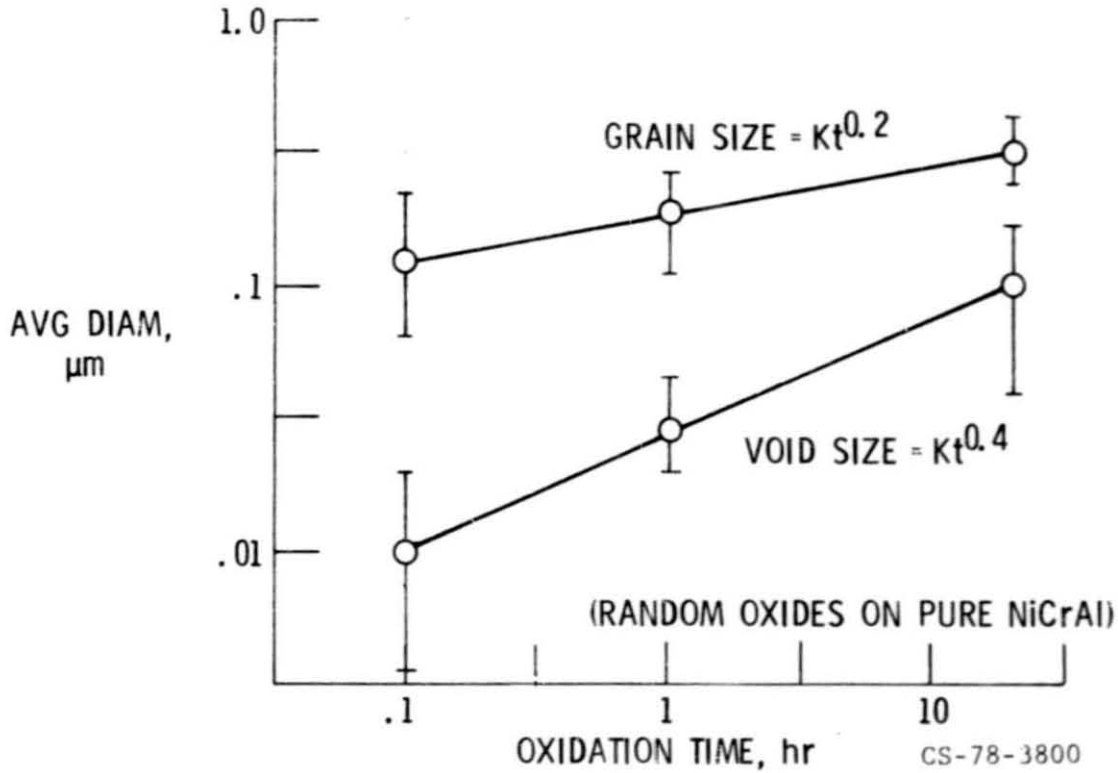

Figure 4. - Kinetics of grain growth and void growth for α-Al_2O_3 scales (near the oxide-gas interface).

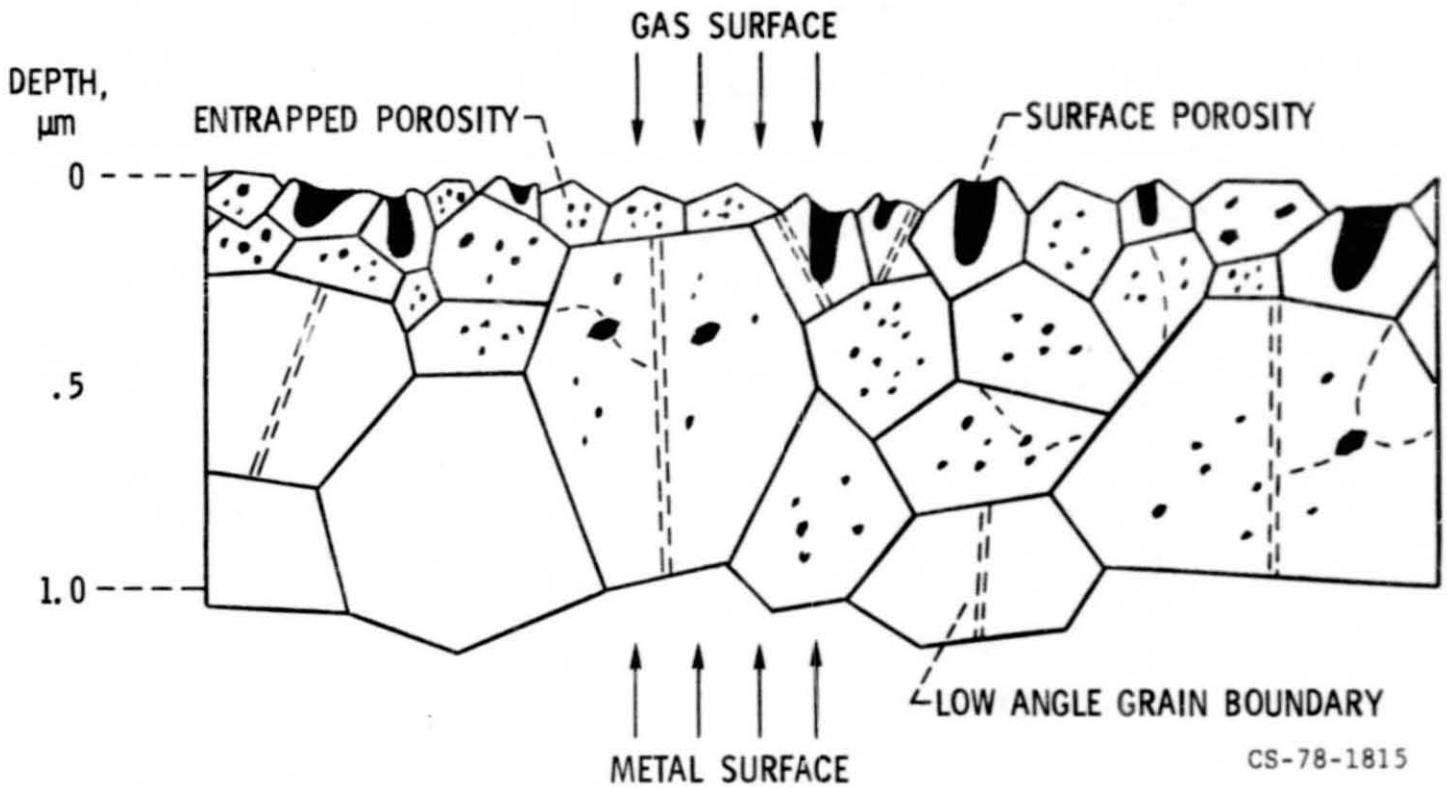

Figure 5. - Schematic cross-section of α-Al_2O_3 scale formed on pure NiCrAl after 20 hr at 1100° C.

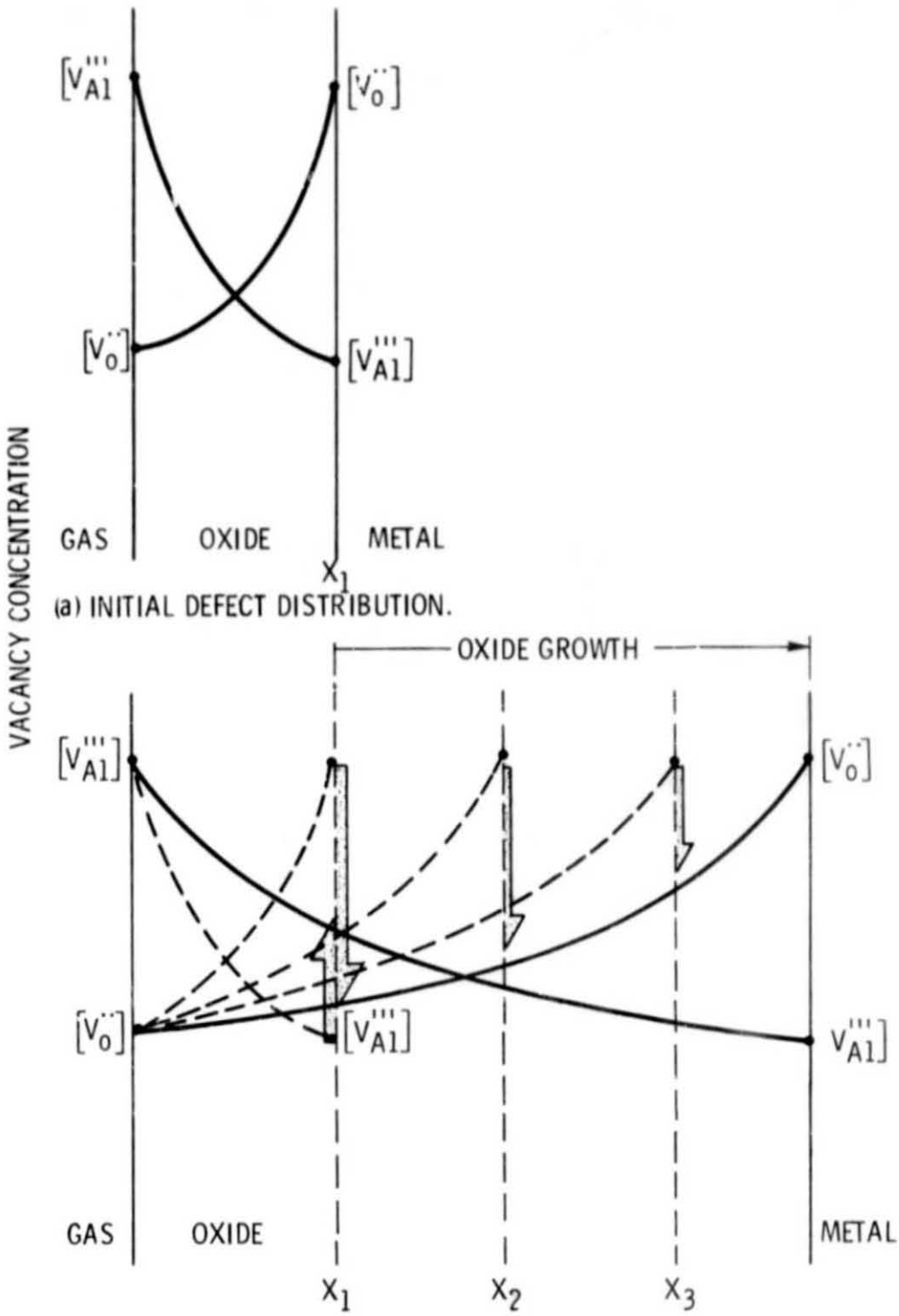

(a) INITIAL DEFECT DISTRIBUTION.

(b) DEFECT DISTRIBUTION AFTER FURTHER OXIDATION (ARROWS SHOW DECREASE IN $[V^{\cdot\cdot}_{O}]_{equilibrium}$ WITH SCALE GROWTH).

Figure 6. - Changes in equilibrium defect concentrations with oxide growth for an inward growing scale.

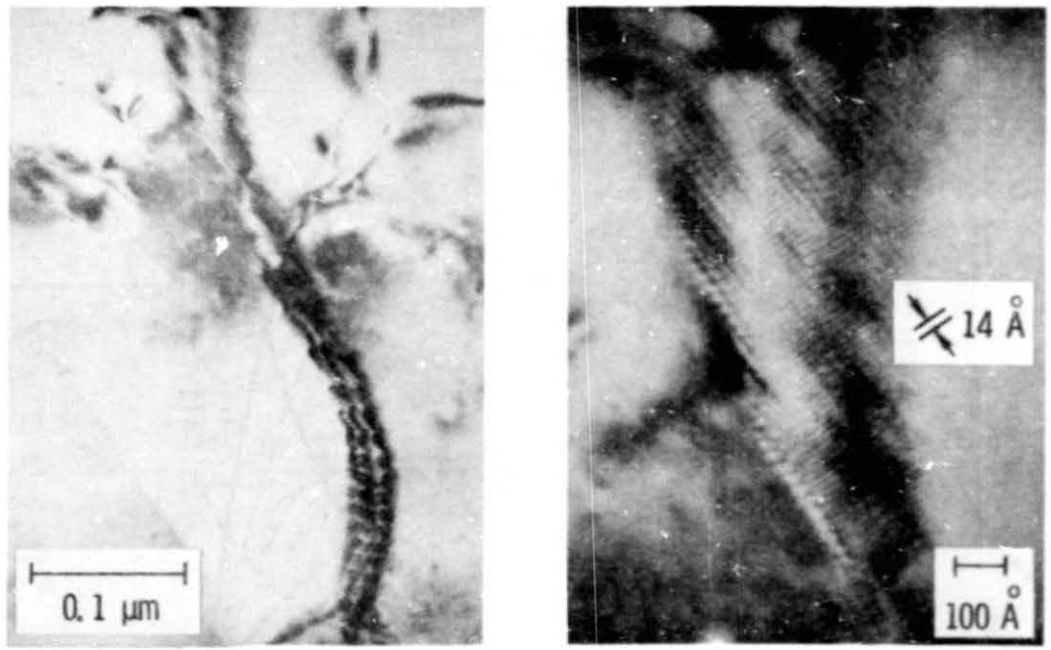

CS-78-1799

Figure 7. - Moire' pattern arising from a low angle grain boundary bisecting an α - Al_2O_3 grain. (Pure NiCrAl oxidized 20 hr at 1100^{o} C.)

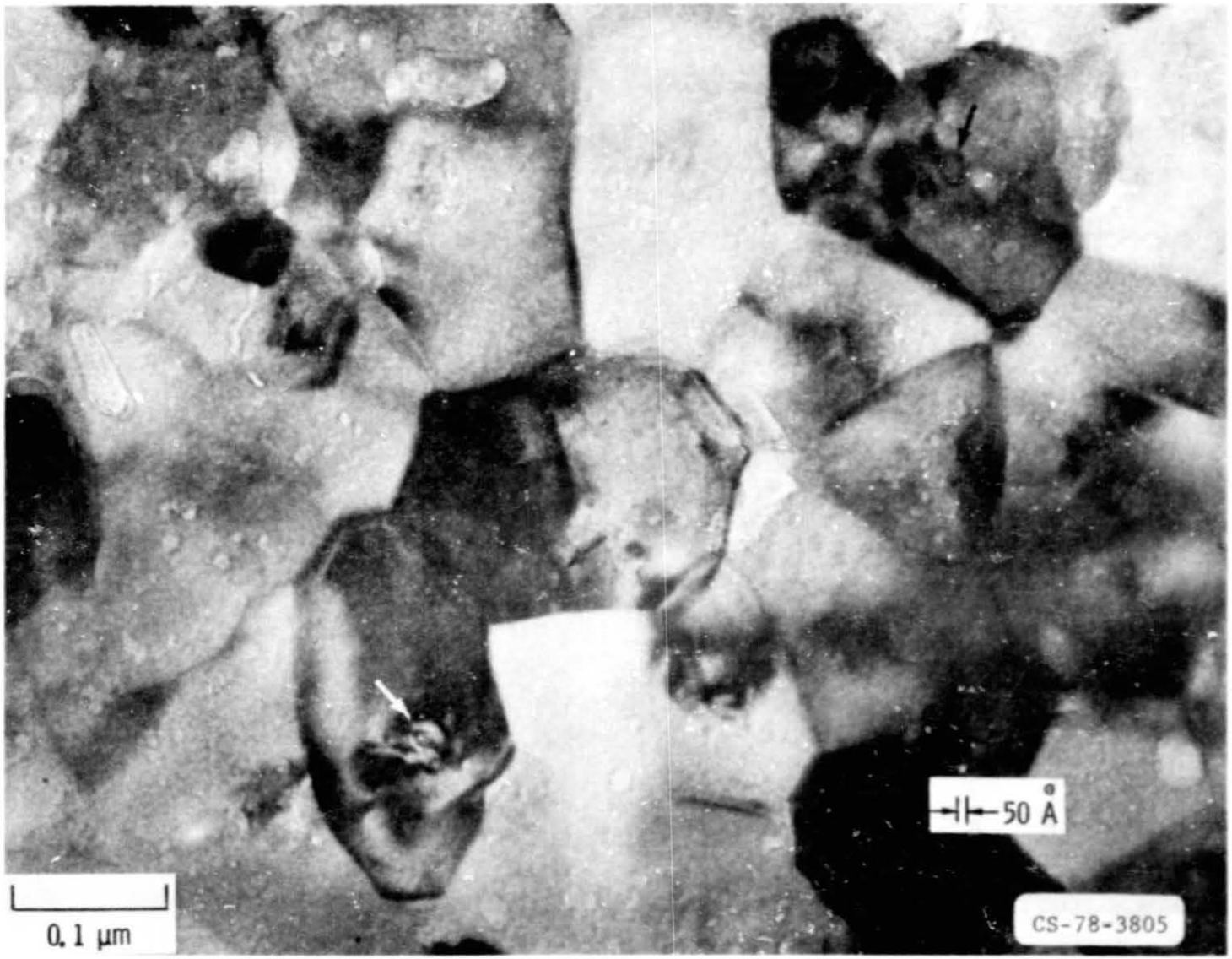

Figure 8. - Fine porosity and strain contrast in a random α - Al_2O_3 scale. (Pure NiCrAl, 0.1 hr, 1100^0 C.)

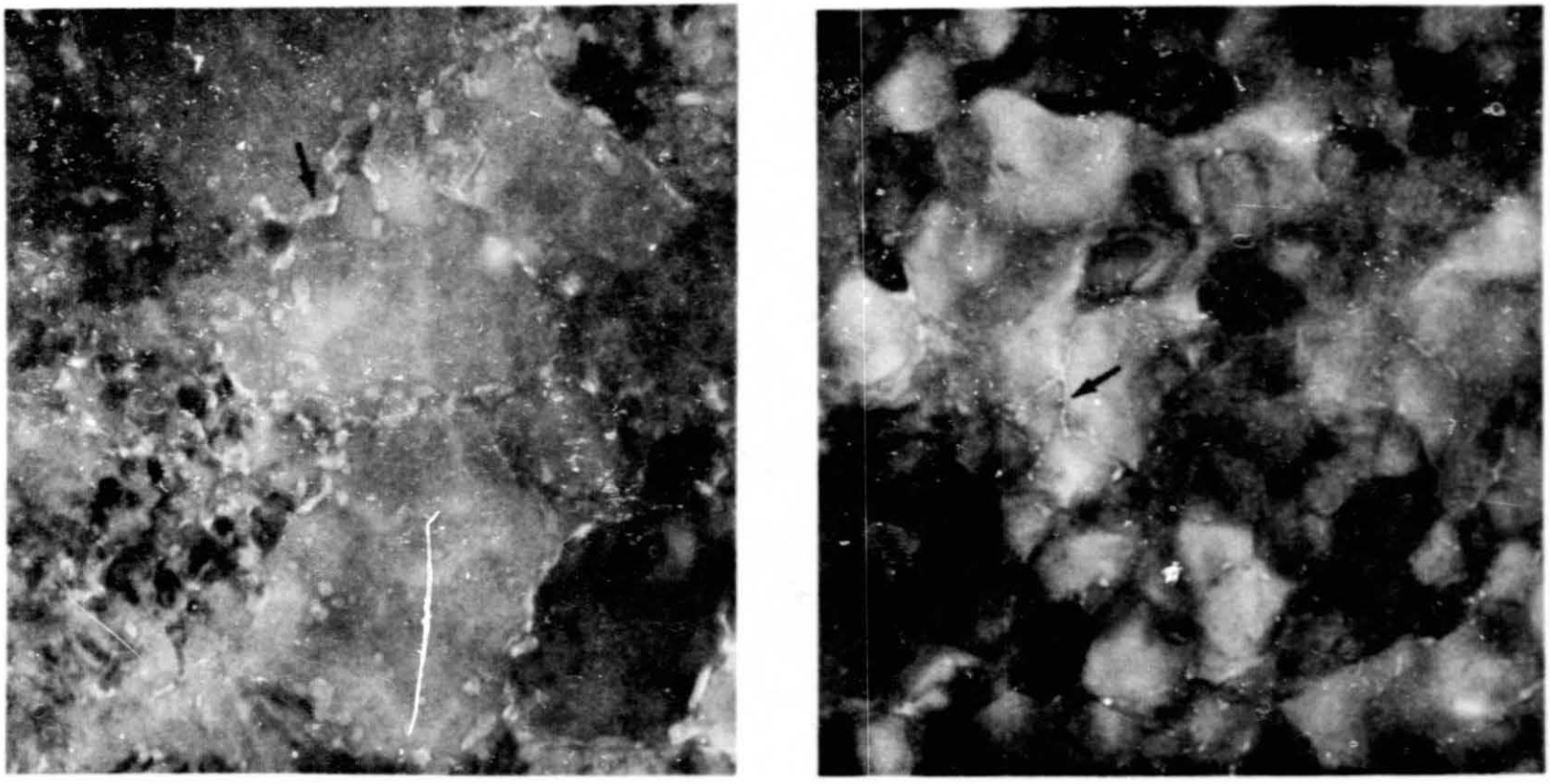

Figure 9. - Grain boundary porosity in α - Al_2O_3 scales on Y-doped NiCrAl, 0.1 hr, 1100° C.

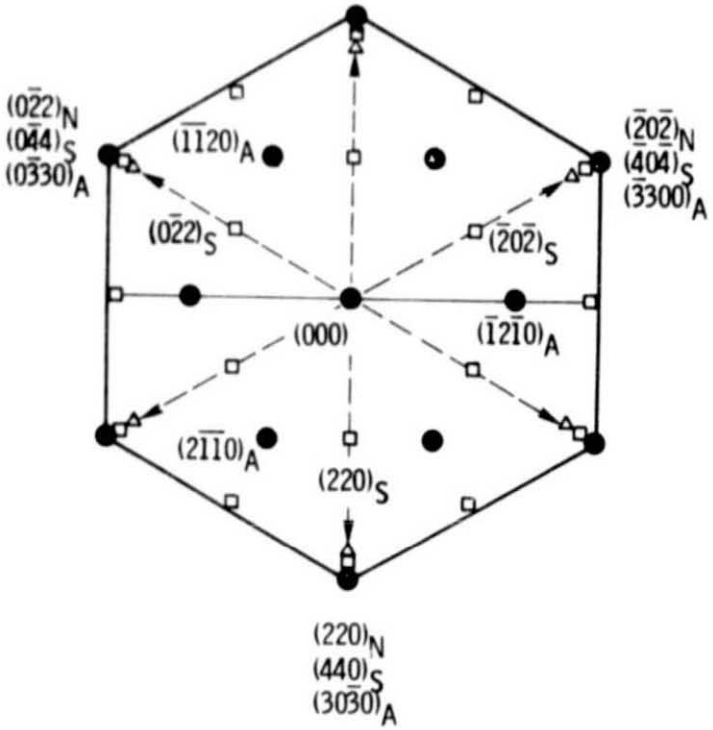

COINCIDENCE OF ORIENTED [0001] Al_2O_3, [$\bar{1}11$] $NiAl_2O_4$, & [$\bar{1}11$] NiO DIFFRACTION PATTERNS

- ● α-Al_2O_3 (A)
- □ $NiAl_2O_4$ SPINEL (S)
- △ NiO (N)
- ←– – CLOSE PACKED ANION DIRECTIONS

(a) CALCULATED PATTERNS SHOWING COINCIDENCE OF ORIENTED [0001] α - Al_2O_3, [$\bar{1}11$] $NiAl_2O_4$, AND [$\bar{1}11$] NiO.

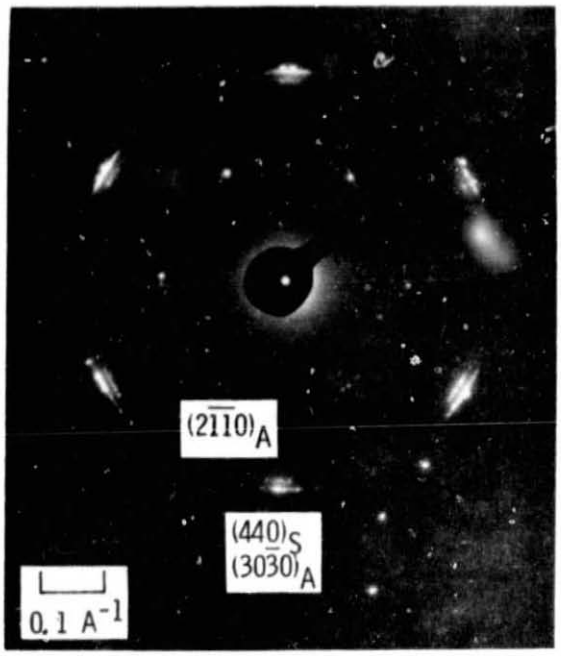

OBSERVED Al_2O_3 - $NiAl_2O_4$ COINCIDENCE
(0001) || {111}
<10$\bar{1}$0> || <110>

CS-78-3812

(b) OBSERVED PATTERNS SHOWING [0001] α - $(Al, Cr)_2O_3$ and [$\bar{1}11$] $Ni(Al, Cr)_2O_4$ COINCIDENCE.

Figure 10. - Analysis of oriented oxide layers formed on Y-doped NiCrAl, 0.1 hr at 1100^0 C.

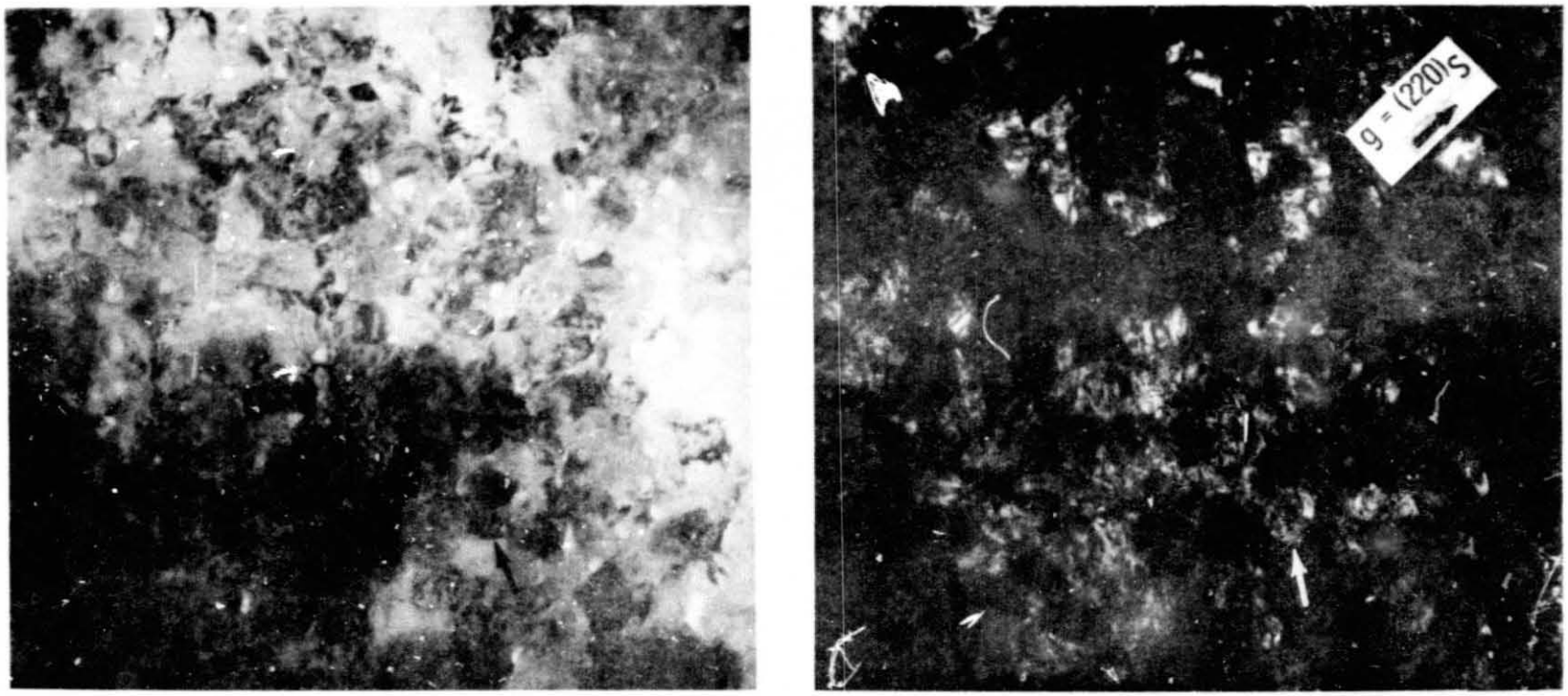

CS-78-3803 (a) BRIGHT FIELD. 0.1 μm (b) DARK FIELD; $\hat{g}$ $(220)_S$, $\hat{B} \sim [1\bar{1}2]_S$.

Figure 11. - Bright field - dark field pair showing subgrains in an oriented γ - Al_2O_3 scale on Zr-doped NiCrAl, 0.1 hr at 1100^0 C.

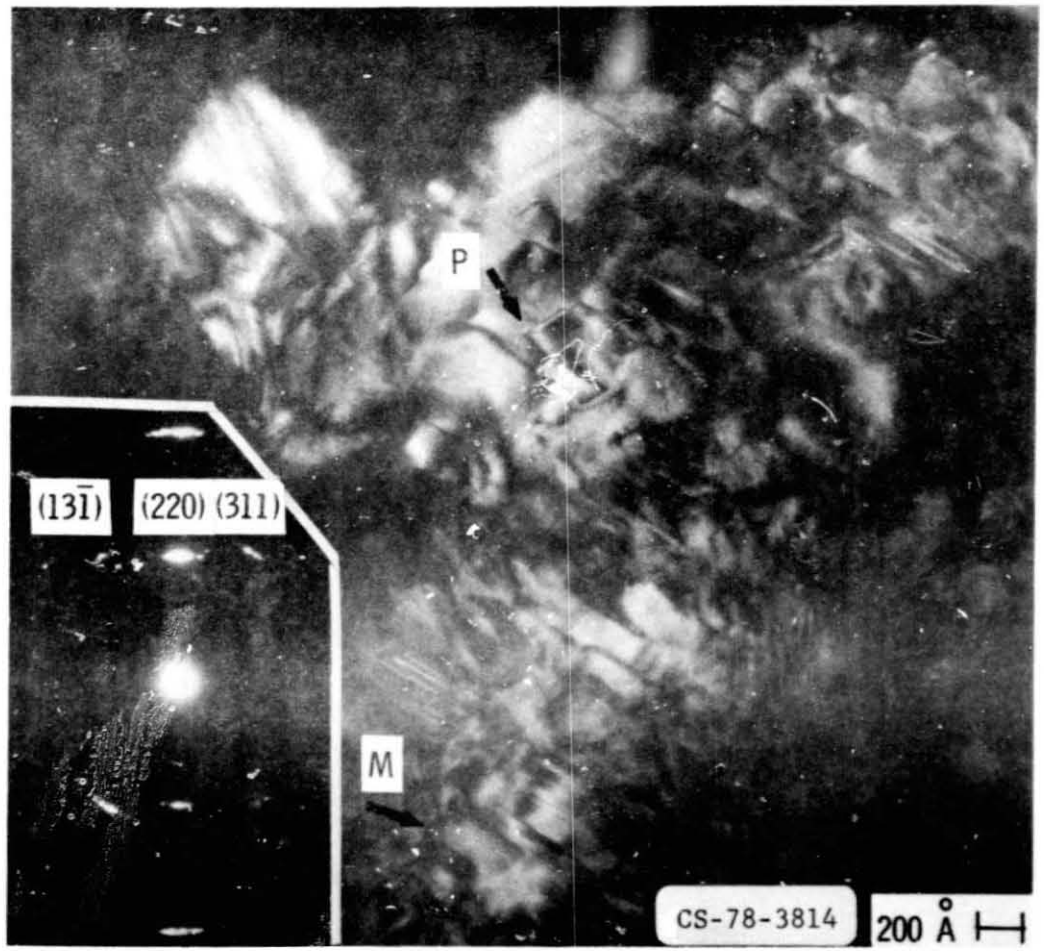

Figure 12. - <110> wiominstatten precipitate in oriented α - Al_2O_3 scale formed on Zr-doped NiCrAl, 0.1 hr at 1100° C; dark field, $\vec{g}$ = (220), $\vec{B}$ = [1$\bar{1}$2]).

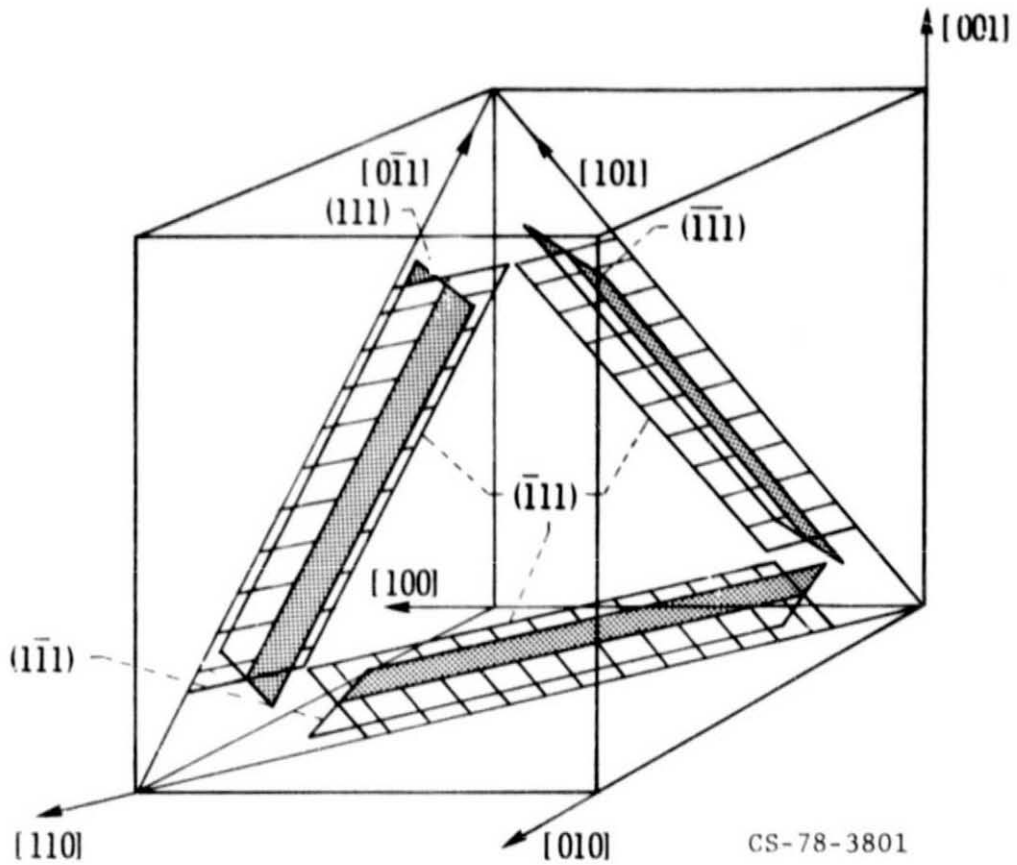

Figure 13. - Proposed {111}⟨110⟩ needle morphology of fine precipitates in oriented γ-Al_2O_3 scale formed on Zr-doped NiCrAl. (0.1 hr, 1100° C)

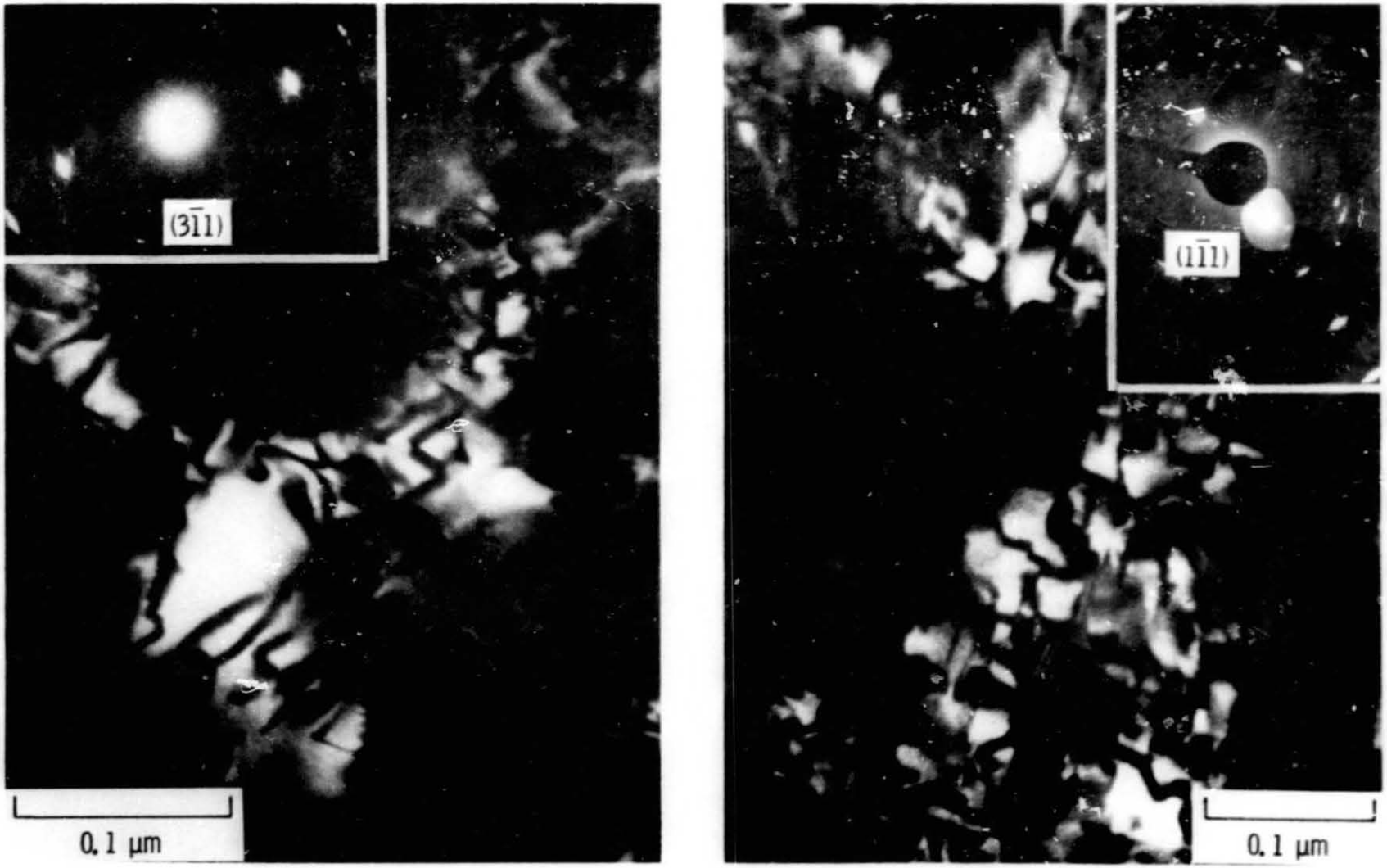

(a) DARK FIELD, g = (3$\bar{1}$1).

(b) DARK FIELD, g = (1$\bar{1}$1). CS-78-3806

Figure 14. - Antiphase domain boundaries in oriented γ - Al_2O_3 scale formed on Zr-doped NiCrAl, 0.1 hr at 1100° C.

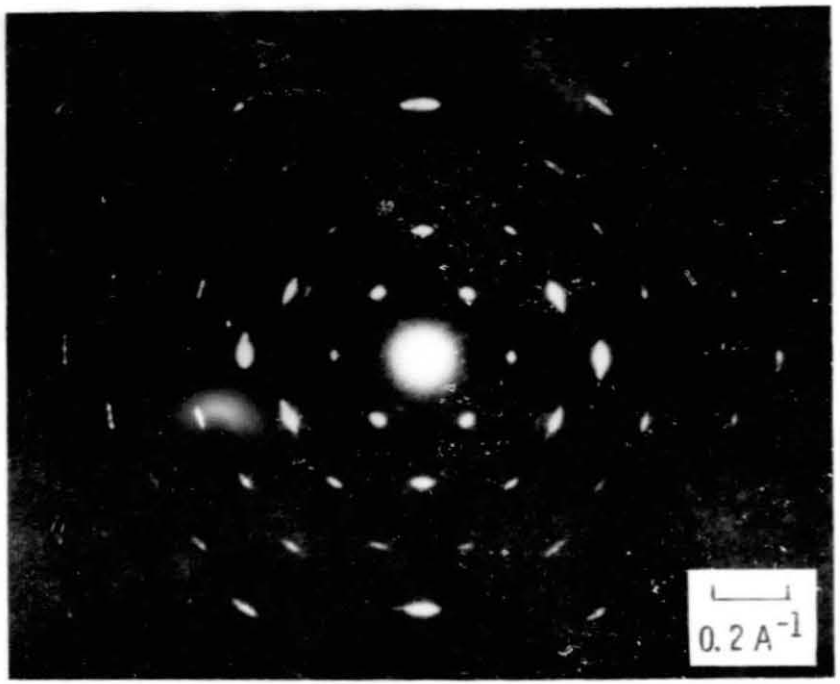

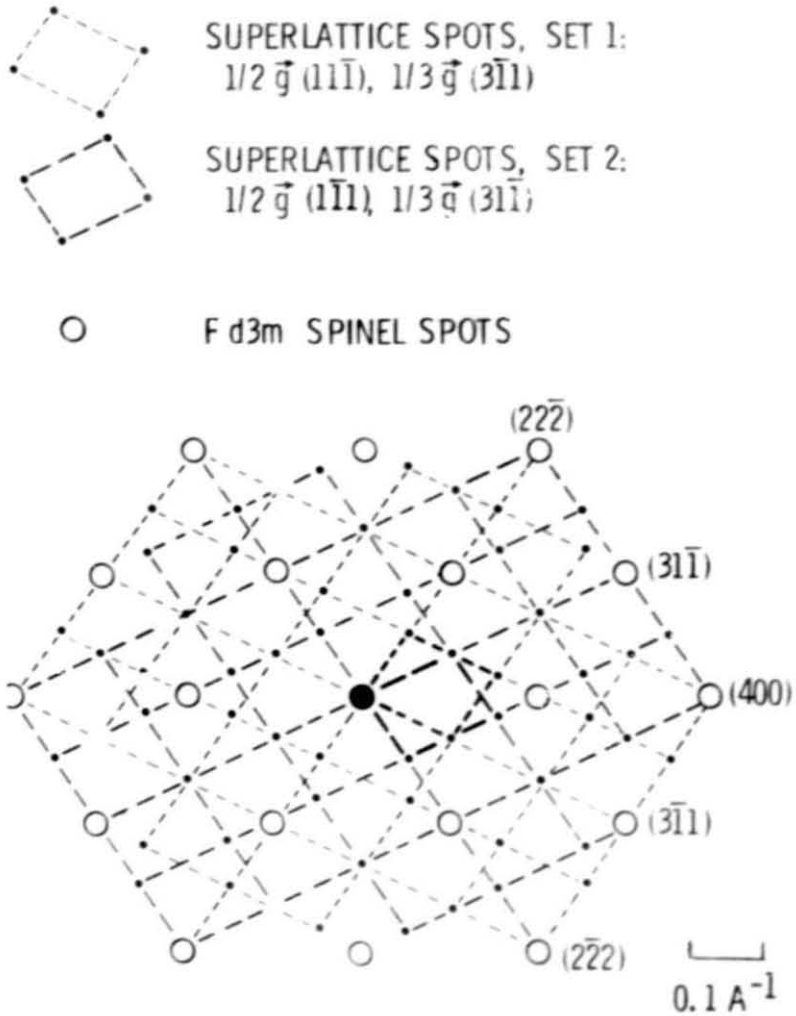

Figure 15. - Superlattice reflections in an [011] zone of the oriented γ - Al_2O_3 scale formed on Zr-doped NiCrAl, 0.1 hr at 1100^{0} C.

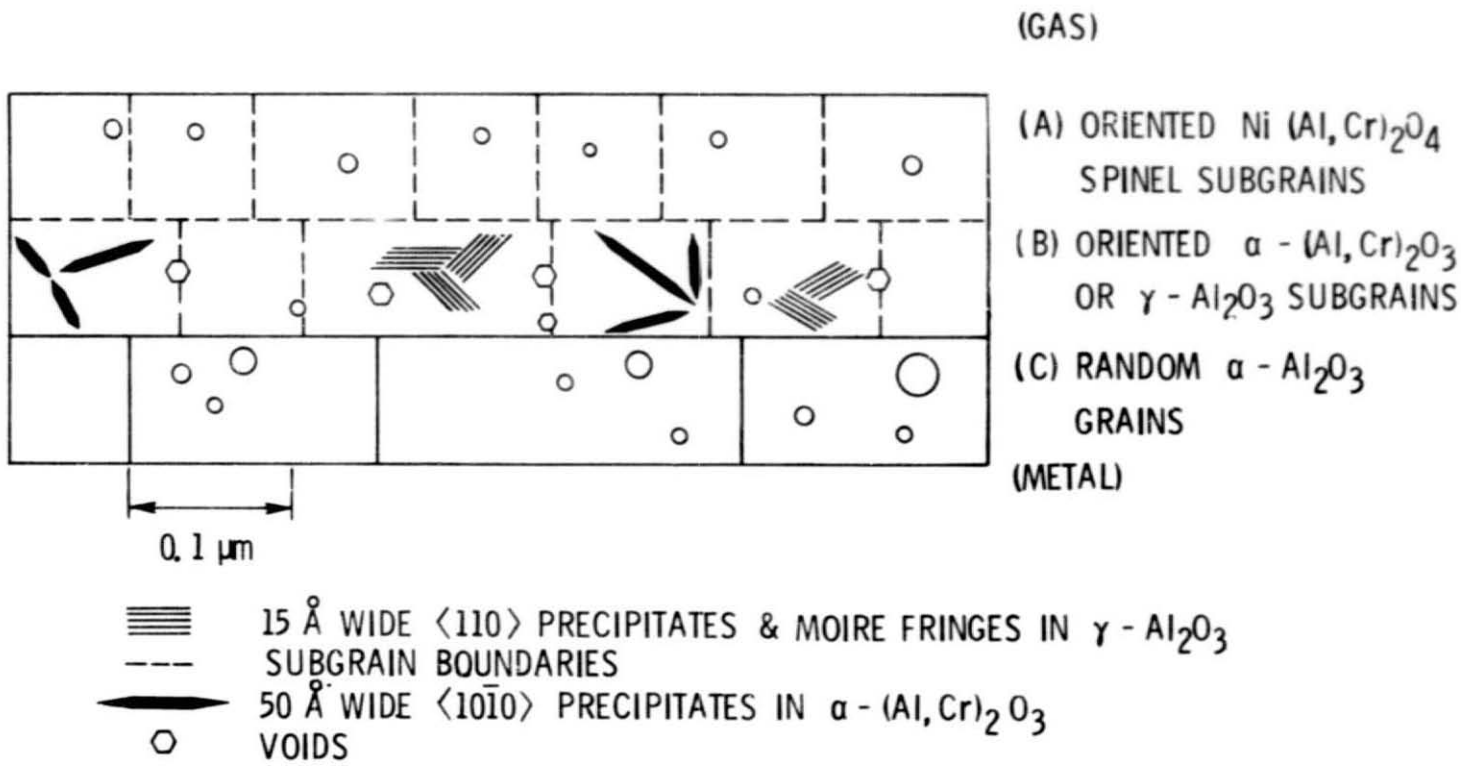

Figure 16. - Possible sequence of transient oxide layers formed on NiCrAl alloys after 0.1 hr at 1100° C.